Real-time Cherenkov emission portal imaging during CyberKnife® radiotherapy

Roussakis, Yiannis; Zhang, Rongxiao; Heyes, Geoff ; Webster, Gareth ; Mason, Suzannah; Green, Stuart; Pogue, Brian; Dehghani, Hamid

DOI:
10.1088/0031-9155/60/22/N419

Real-time Cherenkov emission portal imaging during CyberKnife® radiotherapy

2015 Phys. Med. Biol. 60 N419

(http://iopscience.iop.org/0031-9155/60/22/N419)

OPEN ACCESS
IOP Publishing | Institute of Physics and Engineering in Medicine Physics in Medicine & Biology
Phys. Med. Biol. **60** (2015) N419–N425 doi:10.1088/0031-9155/60/22/N419

Note

Real-time Cherenkov emission portal imaging during CyberKnife® radiotherapy

Yiannis Roussakis[1], Rongxiao Zhang[2], Geoff Heyes[3], Gareth Webster[3], Suzannah Mason[1], Stuart Green[3], Brian Pogue[4] and Hamid Dehghani[1,5]

[1] Physical Sciences of Imaging in the Biomedical Science, University of Birmingham, Birmingham, West Midlands B15 2TT, UK
[2] Department of Physics and Astronomy, Dartmouth College, NH 03755, USA
[3] Medical Physics, Queen Elizabeth Hospital, Queen Elizabeth Medical Centre, Birmingham, UK
[4] Thayer School of Engineering, Dartmouth College, NH 03755, USA
[5] School of Computer Science, University of Birmingham, Birmingham, UK

E-mail: h.dehghani@cs.bham.ac.uk

Received 4 September 2015
Accepted for publication 25 September 2015
Published 29 October 2015

Abstract

The feasibility of real-time portal imaging during radiation therapy, through the Cherenkov emission (CE) effect is investigated via a medical linear accelerator (CyberKnife®) irradiating a partially-filled water tank with a 60 mm circular beam. A graticule of lead/plywood and a number of tissue equivalent materials were alternatively placed at the beam entrance face while the induced CE at the exit face was imaged using a gated electron-multiplying-intensified-charged-coupled device (emICCD) for both stationary and dynamic scenarios. This was replicated on an Elekta Synergy® linear accelerator with portal images acquired using the iViewGT™ system. Profiles across the acquired portal images were analysed to reveal the potential resolution and contrast limits of this novel CE based portal imaging technique and compared against the current standard. The CE resolution study revealed that using the lead/plywood graticule, separations down to 3.4 ± 0.5 mm can be resolved. A 28 mm thick tissue-equivalent rod with electron density of 1.69 relative to water demonstrated a CE contrast of 15% through air and 14% through water sections, as compared to a corresponding contrast of 19% and 12% using the iViewGT™ system. For dynamic scenarios, video rate imaging with 30 frames per second was achieved. It is demonstrated that CE-based portal imaging is

feasible to identify both stationary and dynamic objects within a CyberKnife® radiotherapy treatment field.

Keywords: Cherenkov imaging, portal imaging, radiotherapy, CyberKnife, electronic portal imaging device

S Online supplementary data available from stacks.iop.org/PMB/60/N419/mmedia

(Some figures may appear in colour only in the online journal)

1. Introduction

Cherenkov radiation is emitted when charged particles travel faster than the speed of light in a given dielectric medium (Cerenkov 1934). During x-ray radiotherapy, secondary electrons are predominantly generated from Compton scattering, which have sufficient energy to produce Cherenkov emission (CE) in water or tissue. CE has been shown to be measurable with an optical imaging system, given that the main wavelength of emission is within the visible spectrum and shown to be proportional to radiation doses deposited in the medium (Glaser *et al* 2014).

The incorporation of Cherenkov emission in electronic portal imaging device (EPID) detectors has recently been investigated (Mei *et al* 2006), while Cherenkov radiation imaging has been utilised as a dosimetry technique during photon (Jang *et al* 2012, Zhang *et al* 2013c, Glaser *et al* 2013a, 2013b), electron (Zhang *et al* 2013a, Helo *et al* 2014b) and proton (Helo *et al* 2014a) radiotherapy. Furthermore, real-time superficial dosimetry has been demonstrated in both animal and human studies (Zhang *et al* 2013b, Jarvis *et al* 2014).

In radiotherapy, EPID-based portal imaging is often employed for pre-treatment patient positioning or intra-fraction tumour tracking. While some commercial linear accelerators incorporate portal imaging equipment, the CyberKnife® system does not offer such an option and therefore alternative techniques are desirable. However, due to the fact that the CyberKnife® system utilises multiple non-coplanar and non-isocentric beams, a conventional portal imaging device would not be practicable.

In this study the feasibility of real-time CE portal imaging during CyberKnife® radiotherapy is investigated. This would enable real-time verification of in-patient targeting and treatment delivery accuracy.

2. Methods

A medical linear accelerator (CyberKnife®, Accuray, Sunnyvale, CA) irradiated a partially filled water tank (300 × 300 × 350 mm) using a 60 mm diameter circular beam of 6 MV nominal energy at 800 mm source-axis-distance (SAD) with a dose rate of 10 Gy min^{-1} at a depth of 15 mm. A number of attenuating materials were placed on a moving platform between the beam source and the water tank (figure 1(a)), while an opaque 10 mm thick white solid water slab (Solid Water HE, Gammex Inc, Middleton, WI) was placed at the beam exit face to ensure that only the CE due to radiation at the exit face is imaged. The use of a water slab is in this case (due to the transparent nature of water) critical to ensure that the imaged CE as emitted by the x-ray beam is that of the exit beam. A gated electron-multiplying-intensified-charged-coupled device (emICCD) (PI-MAX4: 512 EM, Princeton Instruments) with a commercial lens (Canon EF 135 mm *f*/2L USM) positioned at the exit face at a small incident angle (~20° to reduce direct radiation to the camera as it was not shielded) imaged the induced CE at the

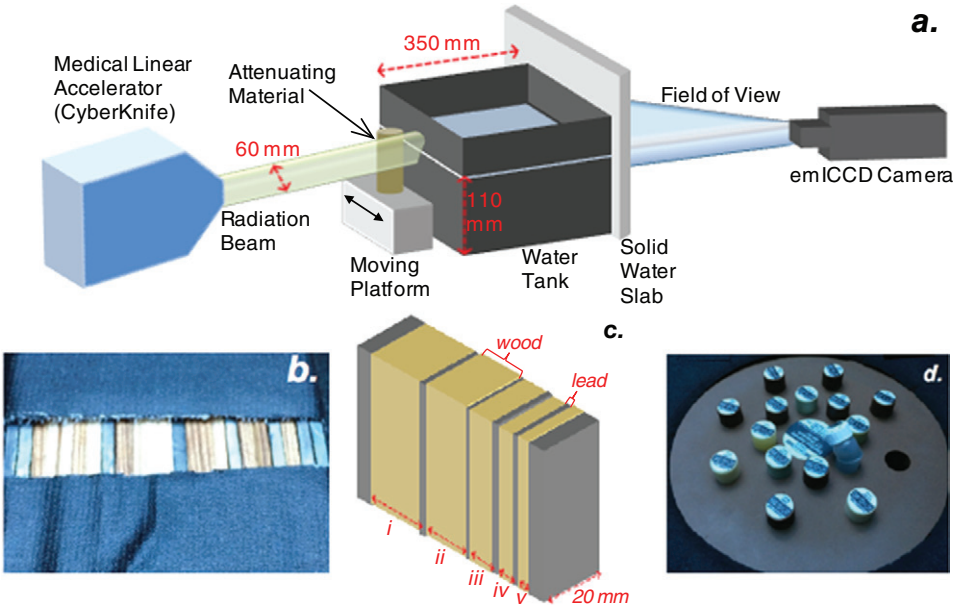

Figure 1. (a) Schematic diagram of the experimental setup; (b) lead/plywood graticule with (c) its corresponding schematic, and (d) tissue equivalent rods (RMI phantom).

surface of the solid water slab. Image acquisition was synchronised with the beam pulses using the trigger signal from the accelerator in order to maximise the signal-to-background ratio (Glaser *et al* 2012).

A number of attenuating materials were used to assess the resolution and contrast of the measured CE at the exit face. For assessment of the resolution a graticule was constructed from a number of lead sheets ($2 \times 60 \times 20$ mm) spaced at regular intervals using plywood separators, figure 1(b). Note that the two lead markers at either end contained two sheets, and therefore represent a thickness of 4 mm. To assess the contrast of the measured CE a number of 28 mm diameter tissue equivalent rods (RMI 467 phantom, Gammex Inc, Middleton, WI) were used, figure 1(d).

The water tank was filled with tap water to a depth of 110 mm, and the phantoms were placed such that the lower 50% of the radiation beam travelled through the phantom and the water, whereas the upper 50% of the beam travelled through the phantom and air, before being measured at the exit face through the solid water slab. CE images were acquired at 30 frames per second (fps) with each frame accumulating CE for 5 radiation pulses. All data were background-subtracted using images with no radiation. The background-subtracted images (30 frames for static and 3 frames for the dynamic) were then median-filtered to produce the CE images for data analysis.

CE-based static and dynamic portal images were visually inspected for an initial proof-of-concept validation. Resolution and contrast were assessed by analysing the profile plots through the two regions of the static images (air and water), facilitating quantitative evaluation. Resolution was quantified by measuring the distances of the minima in the profile plots, associated with the position of the lead sheets. To measure relative contrast, the mean percentage decrease of signal in the profile plots due to the presence of the tissue equivalent rods was calculated with respect to the normalised maximum. Specifically, the mean values for a width of 10 mm centred at the peak/trough of the maximum and minimum values were used.

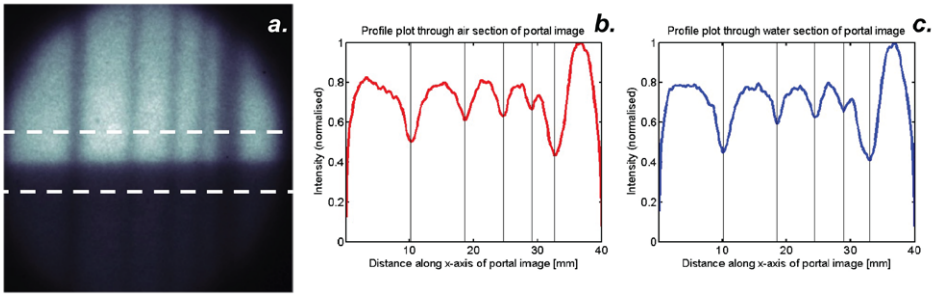

Figure 2. (a) Cherenkov emission image of the graticule phantom acquired from the beam exit face: the white dashed lines represent the profiles used to calculate the contrast for the radiation travelling through (b) water and (c) air.

Table 1. The actual and measured distances between lead sheets from resolution graticule phantom.

		Recovered [mm]	
	Actual [mm]	Air	Water
i	10.40	10.60	10.80
ii	8.80	8.50	8.42
iii	6.00	6.00	5.92
iv	4.40	4.42	4.58
v	3.40	3.58	3.92

The experimental configuration for contrast assessment in static configuration was replicated on an Elekta Synergy® (Elekta AB, Stockholm, Sweden) linear accelerator with portal images being acquired using the iViewGT™ system, to allow direct comparison of CE-based portal imaging against current technology. For this experiment a 240 × 240 mm square beam of 6 MV nominal energy at a dose rate of 3.6 Gy min^{-1} at 1000 mm SAD was employed, with portal images captured for 50 monitor unit (or 0.33 Gy to 1000 mm SAD) acquisitions.

3. Results

A Cherenkov image using the stationary graticule is shown in figure 2 along with profile plots of the measured CE intensity. The intensity profiles through both air and water are self-normalised to allow quantitative analysis of the detected resolution, corresponding to the distance between each lead sheet, figures 2(b) and (c) and table 1. The lowest separation of 3.40 mm (spacing 'v' in figure 1(c)) is clearly evident in the portal image (figure 2(a)) and is measured as 3.58 mm and 3.92 mm for radiation travelling through air and water, respectively. Larger errors are observed at the two edges of the detected signal, which is primarily due to data capture geometry and beam divergence. Each lead sheet with a width of 2 mm is visible (except those at the edges which have a width of 4 mm), highlighting the potentials of higher resolution imaging.

Portal images in the presence of tissue equivalent rods were analysed and the intensity profiles used to assess the measurable relative contrast for each phantom. Figure 3 shows example portal images of the 'SB3 Cortical Bone' phantom as well as the corresponding self-normalised profile plots.

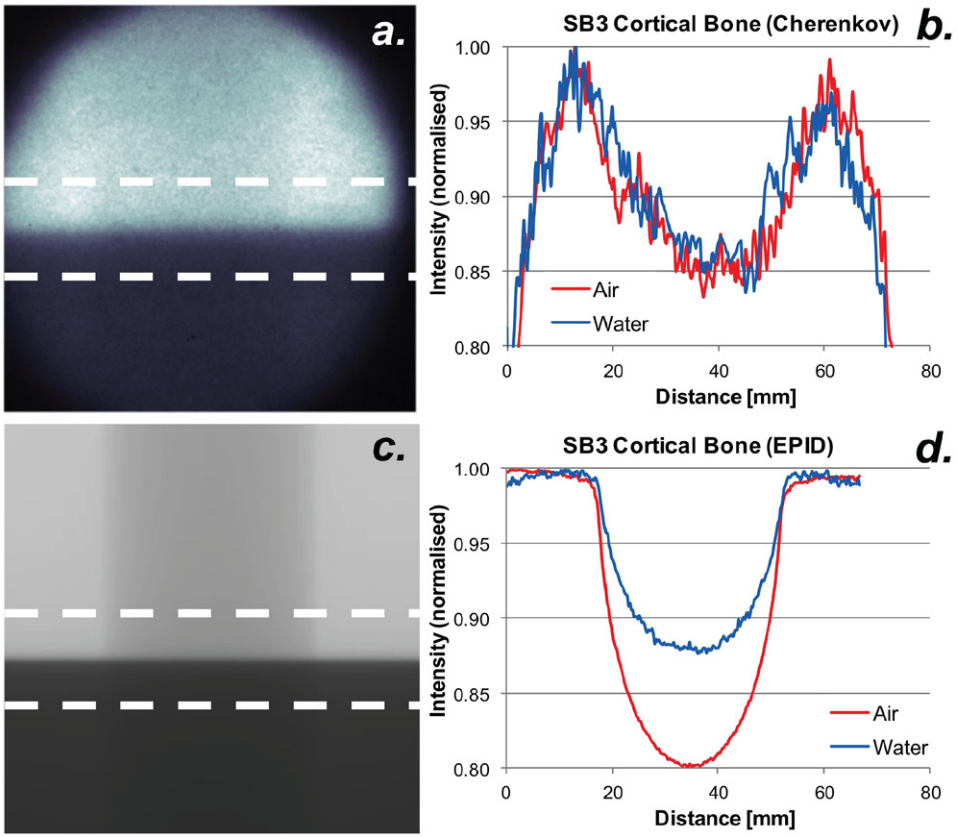

Figure 3. (a) Cherenkov emission portal image of the 'SB3 Cortical Bone' tissue equivalent rod with (b) the associated normalised profile plots; (c) EPID-based portal image of the same tissue equivalent rod with (d) the associated normalised profile plots. The dotted lines in a and c represent the cross-section at which profiles were calculated.

Table 2. Properties of tissue equivalent rods together with the relative Cherenkov emission (CE) and EPID-based portal image contrast.

Name of tissue equivalent rod	Electron density relative to water	Relative CE contrast [%]		Relative EPID contrast [%]	
		Air	Water	Air	Water
SB3 cortical bone	1.69	15	14	19	12
CB2—50% $CaCO_3$	1.47	12	11	16	10
CB2—30% $CaCO_3$	1.28	10	10	15	8
B200 bone mineral	1.10	9	10	13	8
IB inner bone	1.09	8	10	13	8
BRN-SR2 brain	1.04	9	8	12	7

The use of tissue equivalent phantoms demonstrates that CE emission detected at the exit face is sensitive to small contrasts often seen in biological tissue. As summarised in table 2, for tissue equivalent rods with 28 mm diameter, a contrast in CE of up to 15% was observed with an electron density of 1.69 relative to water, with similar contrast seen for beam passing

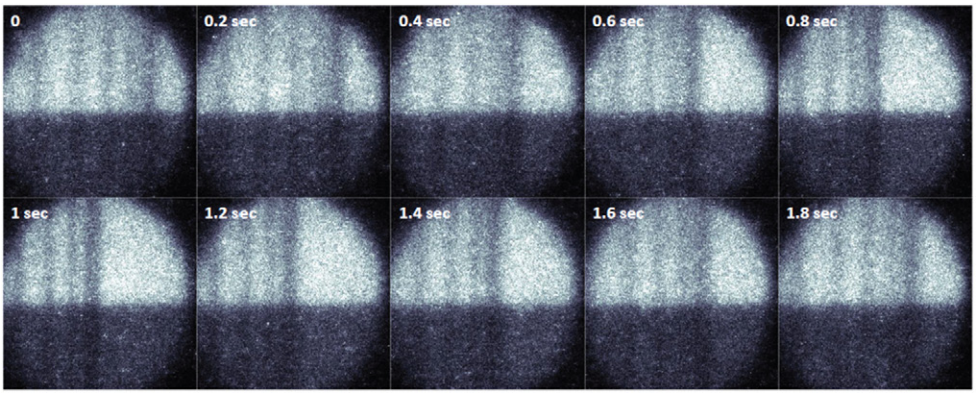

Figure 4. A snap-shot of real-time video (30 fps) CE imaging of a moving graticule.

through the air and water-filled part of the water tank. On the other hand, EPID based portal images revealed higher contrast for beam travelling through the air part of the water tank, with lower contrast for beam travelling through the water-filled part.

Real-time video (30 fps) CE imaging of a moving graticule and a tissue equivalent rod can be seen in the supplementary material (stacks.iop.org/PMB/60/N419/mmedia), with a snapshot shown in figure 4. Even though of inferior image quality due to the substantially lower number of frames in each median-filtered stack, the periodic movement (0.25 Hz) of the phantoms can be observed.

4. Discussion and conclusions

The use of CE for entrance dose measurements have previously been demonstrated showing a direct correlation between measured CE intensity and applied dose. However the use of CE based portal imaging, directly from the exit face of an irradiated medium has not been previously examined.

The use of CE based portal imaging has been demonstrated here, using both a highly attenuating resolution phantom as well as tissue mimicking phantoms. It has been shown that objects with as little as 3.4 mm separation are easily detected, while tissues with relative electron density of greater than 4% (with respect to water) demonstrate CE contrast of 8% or greater. Although the data from the CE based portal images show more noise, this can be overcome through the use of more optimised imaging setup, including the number of measured frames, a more adequate lens and noise removing image processing. Video rate CE based portal imaging was achieved to monitor movements of the graticule and tissue equivalent phantom in real-time. Therefore, CE based portal imaging, a novel imaging technique during radiation therapy, can be potentially applied for systems that lack alternative options such as EPID.

Contrary to EPID-based portal imaging, CE portal imaging only utilizes visible optical photons produced at the exit surface through the CE effect. This minimizes the contribution of scattered radiation (where the scattered photons are at lower energy so are less efficient at producing CE than the transmitted 'primary' beam), resulting in higher measured contrast when radiation passes through water or tissue (as compared to EPID-based portal image), which highlights for the first time the additional benefits of CE portal imaging over EPID-based techniques.

This demonstration of CE based portal imaging can be potentially useful in many applications. Given that the use of CE for detection of entrance and exit dose has been demonstrated, this current work indicates that this method could also be used to detect small deviations in patient positioning and intra-fraction anatomical movements. This is specifically important for applications with the CyberKnife® system as it does not offer portal imaging equipment capabilities as this system utilises multiple non-coplanar and non-isocentric beams where a conventional portal imaging device would not be practicable.

Acknowledgments

This work was supported by Engineering and Physical Sciences Research Council (EPSRC) grant EP/F50053X/1 funding Physical Sciences of Imaging in Bio-medical Sciences (PSIBS) Doctoral Training Centre and in part by the Norris Cotton Cancer Center Developmental Pilot Project Funds, and the NIH Grant No. R01CA109544.

References

Cerenkov P 1934 Visible light from pure liquids under the impact of gamma-rays *C. R. Acad. Sci. URSS* **3** 451–7

Glaser A K, Davis S C, McClatchy D M, Zhang R X, Pogue B W and Gladstone D J 2013a Projection imaging of photon beams by the Čerenkov effect *Med. Phys.* **40** 012101

Glaser A K, Voigt W H A, Davis S C, Zhang R X, Gladstone D J and Pogue B W 2013b 3D Cerenkov tomography of energy deposition from ionizing radiation beams *Opt. Lett.* **38** 634–6

Glaser A K, Zhang R X, Davis S C, Gladstone D J and Pogue B W 2012 Time-gated Cherenkov emission spectroscopy from linear accelerator irradiation of tissue phantoms *Opt. Lett.* **37** 1193–5

Glaser A K, Zhang R X, Gladstone D J and Pogue B W 2014 Optical dosimetry of radiotherapy beams using Cherenkov radiation: the relationship between light emission and dose *Phys. Med. Biol.* **59** 3789–811

Helo Y, Kacperek A, Rosenberg I, Royle G and Gibson A P 2014a The physics of Cerenkov light production during proton therapy *Phys. Med. Biol.* **59** 7107–23

Helo Y, Rosenberg I, D'souza D, Macdonald L, Speller R, Royle G and Gibson A 2014b Imaging Cerenkov emission as a quality assurance tool in electron radiotherapy *Phys. Med. Biol.* **59** 1963–78

Jang K W, Yoo W J, Moon J, Han K T, Park J Y and Lee B 2012 Measurements of relative depth doses and Cerenkov light using a scintillating fiber-optic dosimeter with Co-60 radiotherapy source *Appl. Radiat. Isot.* **70** 274–7

Jarvis L A, Zhang R X, Gladstone D J, Jiang S D, Hitchcock W, Friedman O D, Glaser A K, Jermyn M and Pogue B W 2014 Cherenkov video imaging allows for the first visualization of radiation therapy in real time *Int. J. Radiat. Oncol. Biol. Phys.* **89** 615–22

Mei X, Rowlands J A and Pang G 2006 Electronic portal imaging based on Cerenkov radiation: a new approach and its feasibility *Med. Phys.* **33** 4258–70

Zhang R X, Fox C J, Glaser A K, Gladstone D J and Pogue B W 2013a Superficial dosimetry imaging of Cerenkov emission in electron beam radiotherapy of phantoms *Phys. Med. Biol.* **58** 5477–93

Zhang R, Gladstone D J, Jarvis L A, Strawbridge R R, Hoopes P J, Friedman O D, Glaser A K and Pogue B W 2013b Real-time *in vivo* Cherenkoscopy imaging during external beam radiation therapy *J. Biomed. Opt.* **18** 110504

Zhang R, Glaser A K, Gladstone D J, Fox C J and Pogue B W 2013c Superficial dosimetry imaging based on Čerenkov emission for external beam radiotherapy with megavoltage x-ray beam *Med. Phys.* **40** 101914